Figure 1. Generation of *GluRζ1*^{flox} mice by homologous recombination in C57BL/6 strain derived ES cells. **A**, Schema of the exons 11–22 region of the *GluRζ1* gene (*GluRζ1*$^{+}$), targeting vector, floxed and *neo*-inserted allele (*GluRζ1*^{flox}; *neo*), and floxed allele (*GluRζ1*^{flox}). Exons 19 and 20 encode the putative transmembrane segment M4 of GluRζ1. The *GluRζ1*^{flox}; *neo* allele contains two *loxP* sequences flanking exons 19 and 20 of the *GluRζ1* gene and the *neo* gene flanked by two *frt* sequences. The *neo* gene was removed *in vivo* by crossing *GluRζ1*$^{+/flox}$; +/*neo* mice with FLP66 mice carrying the Flp recombinase gene under the control of the *EF1α* promoter. *GluRζ1*$^{+/flox}$ mice were crossed with GluRγ1-Cre mice to disrupt the GluRζ1 gene selectively in the hippocampal CA3 region. Abbreviations: BSK, plasmid pBluescript; DT, diphtheria toxin gene; neo, neomycin phosphotransferase gene; E, *Eco*RI; N, *Not*I; S, *Spe*I; X, *Xba*I. Hatched boxes indicate the location of probes for Southern blot analysis. **B**, Southern blot analysis of genomic DNA from *GluRζ1*$^{+/+}$, *GluRζ1*$^{+/flox}$; +/*neo*, and *GluRζ1*$^{+/flox}$ mice. *Eco*RI-digested DNA was hybridized with 3′ probe. **C**, Agarose gel electrophoresis of DNA fragments amplified by PCR from *GluRζ1*$^{+/+}$, *GluRζ1*$^{+/flox}$ and *GluRζ1*$^{flox/flox}$ mice. The amplified DNA fragments derived from the *GluRζ1*$^{+}$ and *GluRζ1*^{flox} alleles were 61 bp and 169 bp, respectively. **D**, Western blot analysis of GluRζ1 and neuron-specific enolase (NSE) proteins in whole-brain homogenates from *GluRζ1*$^{+/+}$ and *GluRζ1*$^{flox/flox}$ mice.
doi:10.1371/journal.pone.0003993.g001

three-dimensional reconstructed image were compared with both the unprocessed, individual optical sections and with a 'movie', in which segments of the three-dimensional reconstruction were rotated around the dendritic axis (IMARIS, Bitplane). For dendritic analysis, neurons were imaged on a Leica SP-5 with a 40×objective (N.A. 0.8). Optical sections were collected at intervals of 2 μm and averaged 8 times. The topographical order of the dendritic tree was made using the semi-automated program FilamentTracer (Bitplane). Analysis of dendritic topology included dendritic branches up to the third order. Analysis of dendritic spines was performed in rather linear, apical secondary and tertiary dendrites.

In situ hybridization

Isotopic detection of mRNAs was performed as described [32]. All samples were subjected to hybridization analysis at the same time and sections were exposed to a single x-ray film for measurement of relative optical density with IP Lab software. The relative expression levels of the mRNAs in the hippocampal CA3 region were calculated using the ratio of the density in the CA3 region to that of the CA1 region, except that the *GluRγ1* mRNA density in the CA3 region was directly compared between control and mutant mice. Double *in situ* hybridization was performed with mixture of [^{33}P]dATP-labeled oligonucleotide probe for GluRζ1 (complementary to residues 2583–2627, GenBank accession No. D10028) and digoxigenin (DIG)-labeled cRNA probe for GAD67 (complementary to residues 802–1617, No. A28072) as described [33]. Hybridization signals were visualized with nuclear track emulsion (NTB-2, Kodak) and fluorescent substrate (HNPP Fluorescent Detection Set, Boehringer-Mannheim), respectively. Sections were counterstained with NeuroTrace 500/525 green (Molecular Probes).

Kainate-induced seizure

Kainate was intraperitoneally administered to mice, and they were monitored for 1 h to determine whether they exhibited seizures with generalized tonic-clonic activity accompanying the loss of postural tone. Mice were then fixed under deep pentobarbital anesthesia for immunohistochemical analysis with the c-Fos antibody (Oncogene) 2 h after kainate administration.

Electrophysiology

Transverse hippocampal slices (400 μm thick) were superfused with an artificial cerebrospinal fluid (aCSF) containing (in mM): 119 NaCl, 2.5 KCl, 2.5 $CaCl_2$, 1.3 $MgSO_4$, 1 NaH_2PO_4, 26.2 $NaHCO_3$, and 11 glucose, which was equilibrated with 95% O_2/5% CO_2. Synaptic responses were evoked via a bipolar stimulating electrode placed in the CA3 stratum radiatum and whole-cell recordings were made from CA3 pyramidal cells using the blind-patch technique. The stimulus strength was set at the beginning of each experiment so that the average amplitude of synaptic responses in the absence of any antagonists is around 200 pA at a holding potential of −80 mV. The AMPA receptor-mediated excitatory postsynaptic current (AMPA-EPSC) was isolated by subtracting the synaptic response in the presence of 10 μM 6-cyano-7-nitroquinoxaline-2,3-dione (CNQX) from that in its absence. The NMDA receptor-mediated excitatory postsynaptic current (NMDA-EPSC) was recorded at +50 mV in the presence of 10 μM CNQX and 0.1 mM picrotoxin. The $GABA_A$ receptor-mediated inhibitory postsynaptic current ($GABA_A$-IPSC) was recorded at 0 mV in the presence of 10 μM CNQX and 25 μM D-2-amino-5-phosphonovaleric acid (D-APV). The stimulus strength was constant throughout each experiment. The slow hyperpolarizing currents induced by high-frequency stimulation (50 Hz, 40 pulses) were recorded at −20 mV in the presence of 0.1 mM picrotoxin as described previously [34]. Patch electrodes were filled with an internal solution containing (in mM): 140 potassium methansulfonate, 8 NaCl, 10 HEPES, 2 MgATP, and 0.3 Na_3-GTP (pH 7.2 adjusted with KOH, osmolarity 290 to 300 mOsm). For pharmacological experiments, 10 mM BAPTA was added in the pipette solution or potassium methansulfonate in the pipette solution was replaced by cesium methansulfonate. Voltage-clamped responses were recorded with an Axopatch 1D amplifier (Axon Instruments, Union City, CA, USA) and the signal was filtered at 1 kHz, digitized at 2.5 kHz, and stored on a personal computer.

Field potential recording *in vivo*

Urethane-anesthetized mice (1 g/kg body weight, i.p.) were fixed in a stereotaxic head holder (Narishige). For the recording of local field potentials, a tungsten electrode (2–5 MΩ, Frederick Haer) or a silicon probe (16 recoding sites with 50 μm separation, NeuroNexus Technologies) was inserted into the hippocampal CA3 region (AP = −2.0 mm from bregma, L = ±2.3 mm from midline, and V = +2.0 mm ventral to dura), the hippocampal CA1 region (AP = −2.0, L = ±1.0, V = +1.2) or the dentate gyrus (AP = −2.0, L = ±1.0, V = +2.0). Signals were amplified (MEG-1200, Nihon Kohden), band-pass filtered (0.08–1,000 Hz), digitized at 1 kHz through an AD converter (National Instruments), and stored in a computer. Analyses of data were performed offline using LabVIEW (National Instruments) and IGOR (Wave matics) software. Recordings using a glass electrode (10–15 MΩ, GD-2, Narishige) were carried out as described [35]. Raw traces (0.08–3,000 Hz) were band-pass filtered for the detection of MUA of neurons (0.15–3 kHz). EEG spikes with power of twice the s.d. from the baseline mean and the duration of about 30 ms were extracted. The unit activity was defined as a power of more than five times the s.d. from the baseline mean and the duration of less than 4 ms [7]. The locations of the electrode were verified histologically. CSD analyses were carried out as described [8].

Pharmacological experiments. Mice were anesthetized with ketamine (80 mg/kg, i.p.; Sankyo Co., Tokyo, Japan) and xylazine (20 mg/kg i.p.; Bayer, Tokyo, Japan), and fixed to a

stereotaxic apparatus (David Kopf, Tujunga, CA, USA). Two single guide cannulae (Plastics One, Roanoke, VA, USA) were implanted into the CA3 region of the hippocampus bilaterally (stereotaxic coordinates: AP = −2.2 mm from bregma, ML = ±2.5 mm from midline, DV = +1.4 mm from bregma), according to an atlas of the mouse brain [36]. The tip of the internal cannula for microinjection was inserted 1 mm below the tip of the guide cannulae (DV = +2.4 mm from bregma). The cannulae were fixed to the skull with dental cement. The animals were allowed to recover for at least 5 days. D,L-APV (Sigma-Aldrich, MO, USA) was dissolved in aCSF at a concentration of 30 mM. The aCSF was consisted of NaCl (150 mM), KCl (3 mM), $CaCl_2$ (1.4 mM), $MgCl_2$ (0.8 mM), Na_2HPO_4 (0.8 mM), and NaH_2PO_4 (0.2 mM). During drug infusions, the mice were restrained lightly in the disposable vinyl jacket (Braintree Scientific, Inc, MA, USA) and 0.5 µl of the drug or aCSF was infused at a rate of 0.2 µl/min using a microinjection pump (CMA/100, CMA/Microdialysis, Solna, Sweden). The infusion cannulae (bilateral) were left in place for a further 1 min to diffuse the drug from the needle tip, and the animal was then returned to its home cage. Kainate was delivered i.p. 20–30 min after APV injection.

Statistical analysis

All behavioral experiments were performed in a blind fashion. Data were expressed as mean±SEM. Statistical analysis was performed using Fisher's exact probability test, Kolmogorov-Smirnov test, log-rank test and Student *t*-test as appropriate. Statistical significance was set at $p<0.05$.

Results

Selective ablation of NMDA receptors in hippocampal CA3 pyramidal neurons

We disrupted the NMDA receptor *GluRζ1/NR1* gene specifically in the hippocampal CA3 pyramidal cells by Cre-*loxP* recombination on the C57BL/6N genetic background. By crossing a target mouse line carrying two *loxP* sequences flanking exon 19 and 20 of the *GluRζ1* gene (*GluRζ1*$^{+/flox}$ mice) with a hippocampal CA3 region-dominant Cre mouse line carrying the Cre recombinase gene inserted into the *GluRγ1/KA-1* gene (GluRγ1-Cre mice), we obtained *GluRγ1*$^{+/cre}$; *GluRζ1*$^{flox/flox}$ mice and *GluRζ1*$^{flox/flox}$ mice (Fig. 1), and used them in subsequent experiments as mutant and control mice, respectively.

In situ hybridization signals for the *GluRζ1* mRNA were indistinguishable between mutant and control mice at postnatal day 1 (P1) (Fig. 2A). At P7, *GluRζ1* signals were diminished specifically in the hippocampal CA3 region of mutant mice (Fig. 2B). At P21 to P23, the hybridization signals were hardly detectable in the CA3 region of mutant mice and slightly decreased in the brainstem (Fig. 2C). Residual hybridization signals for the *GluRζ1* mRNA were co-localized with those of the *GAD67* mRNA, suggesting that expression of the *GluRζ1* mRNA was intact in CA3 interneurons (Fig. 2G, $n = 17$ out of 17 GAD67-positive cells). Immunohistochemical analyses showed that immunoreactivity for GluRζ1 protein was present in the CA3 region at P7, though the amount appeared to be decreased (Fig. 2D). However, the expression of GluRζ1 protein was diminished to a negligible level at P14 and P21 (Fig. 2E and F).

We examined NMDA-EPSCs by whole-cell patch-clamp recordings from the pyramidal cell in the CA3 region of the hippocampus at P21 to P23. NMDA-EPSCs were evoked by stimulating associational/commissural fibers that mainly terminate in the stratum radiatum since NMDA receptors are more

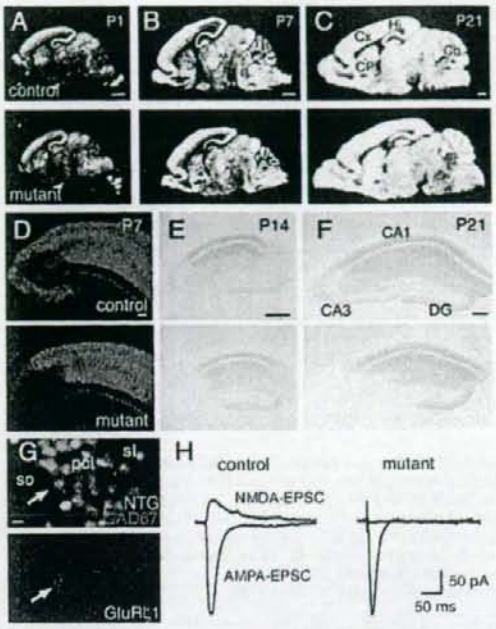

Figure 2. Generation of CA3 pyramidal neuron-selective NMDA receptor knockout mice. A–C, X-ray film autoradiography for *GluRζ1* mRNAs. Arrowheads indicate the CA3 region. **D–F**, Immunohistochemistry for GluRζ1 proteins. **G**, Double *in situ* hybridization for *GluRζ1* (white) and *GAD67* mRNA (red), counterstained with neurotrace green (green), in the mutant CA3 region. Arrow indicates a neuron expressing both *GluRζ1* and *GAD67* mRNAs. Scale bars: **A–C**, 1 mm; **D–F**, 200 µm; **G**, 10 µm. Abbreviations: Cb, cerebellum; CP, caudate-putamen; Cx, cortex; DG, dentate gyrus; Hi, hippocampus; pcl, pyramidal cell layer; sl, stratum lucidum; so, stratum oriens. **H**, Representative traces of AMPA- and NMDA-EPSCs at CA3 commissural/associational synapses.
doi:10.1371/journal.pone.0003993.g002

abundantly expressed in the stratum radiatum than in the stratum lucidum (Fig. 2H). In mutant mice, NMDA-EPSCs were not detectable, while AMPA-EPSCs were normally evoked. The ratios of the amplitudes of NMDA-EPSCs to those of AMPA-EPSCs were 50.9±16.1% (mean±s.e.m.) in control mice and 0.2±0.2% in mutant mice ($n = 4$ each; *t*-test, $P = 0.03$). Thus, NMDA receptors were abolished in hippocampal CA3 pyramidal neurons of mutant mice by P21. We used mutant and control mice at P21 to P23 in the following experiments unless otherwise specified.

Enhanced susceptibility of mutant mice to kainate-induced seizure

To monitor the excitability of CA3 recurrent circuits *in vivo*, we tested the kainate sensitivity of mutant mice since the administration of kainate to rodents stimulates initially the CA3 region and then generates seizures [37]. Intraperitoneal administration of kainate at 8 mg/kg induced tonic-clonic seizures with loss of the postural tone in mutant mice within 1 h, but not in control mice (Fig. 3A, $P<0.001$, Fisher's exact probability test). Mice of both genotypes showed seizures at a higher dosage of kainate (12 mg/kg), but the latency to the onset of seizures was significantly shorter in mutant mice (Fig. 3B, $P = 0.03$, log-rank test). Neither mutant

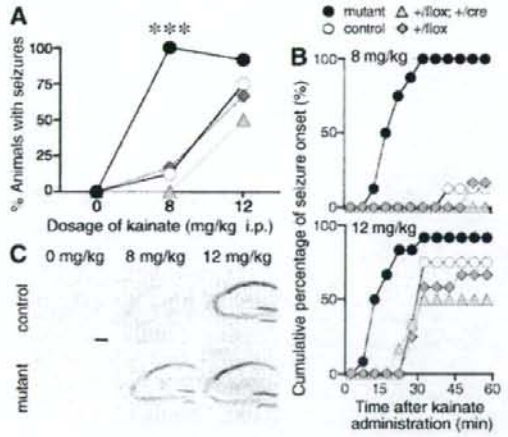

Figure 3. Increased susceptibility to kainate-induced tonic-clonic seizures in the mutant mice. A, The graph represents the percentage of mice with the generalized tonic-clonic seizures 1 h after drug administration. ***, $P<0.001$, Fisher's exact probability test. **B**, Cumulative curves for the onset of seizure. Saline, $n=4$–6; 8 mg/kg, $n=7$–8; 12 mg/kg, $n=12$. **C**, c-Fos immunohistochemistry in the hippocampus. Scale bar, 200 μm.
doi:10.1371/journal.pone.0003993.g003

nor control mice showed seizures after saline-administration. These results suggest that kainate-induced seizure susceptibility was enhanced in mutant mice. Susceptibility to the seizure was comparable between control *GluRζ1*$^{flox/flox}$ mice and *GluRγ1*$^{+/cre}$; *GluRζ1*$^{+/flox}$ mice, indicating that the insertion of the *Cre* gene in one allele of *GluRγ1* locus did not influence the susceptibility.

To monitor the neuronal activity *in vivo*, we employed c-Fos immunohistochemistry. There was little c-Fos immunoreactivity in the hippocampus of both control and mutant mice administrated with saline ($n=3$, Fig. 3C). Administration of kainate at 8 mg/kg induced strong c-Fos-immunoreactivity in the hippocampus of mutant mice ($n=3$). In contrast, no significant immunoreactivity was detectable in the hippocampus of kainate-administrated control mice ($n=3$). Kainate at 12 mg/kg induced strong c-Fos immunoreactivity in both control and mutant mice with seizures, while the number of Fos-immunopositive cells in the hippocampus was significantly smaller in mutant mice than in control mice ($n=20$ sections from 5 mice). The cellular imaging of neural activity with c-Fos immunohistochemistry confirmed the enhanced seizure susceptibility of mutant mice.

Histological features of the hippocampal CA3 region

Unexpectedly, we found that mutant mice lacking NMDA receptors selectively in CA3 pyramidal neurons became more susceptible to kainate-induced seizures. One obvious possibility is that the ablation of NMDA receptors may disturb the neural wiring of the hippocampal CA3 region, leading to abnormal excitability of the network. We thus examined the histological features of the hippocampal CA3 region in detail. The laminar organization and cellular distribution of the hippocampal CA3 region examined by Nissl staining was indistinguishable between control and mutant mice (Fig. 4A). Immunostaining for vesicular glutamate transporter 2 (VGluT2) and calbindin showed that the afferent terminals from the entorhinal cortex and the dentate gyrus were localized in the stratum lacunosum-moleculare and the stratum lucidum in both control and mutant mice, respectively (Fig. 4B and C).

Golgi staining revealed no appreciable differences in dendritic arborization of CA3 pyramidal cells between control and mutant mice (Fig. 4G). There were no significant differences in the numbers of branch points (control, 16.6 ± 1.1, $n=8$; mutant, 17.0 ± 1.1, $n=9$; $P=0.80$; *t*-test) and the primary (control, 4.4 ± 0.5; mutant, 3.8 ± 0.6; $P=0.45$), secondary (control, 7.8 ± 0.7; mutant, 7.0 ± 0.7; $P=0.49$) and tertiary dendrites (control, 9.4 ± 1.4; mutant, 9.9 ± 1.0; $P=0.76$) between two genotypes (Fig. 4I and J). Mean spine density on basal dendrites of CA3 pyramidal cells was also comparable ($n=28$ dendrites from 3–4 mice, $P=0.15$) (Fig. 4H and K). Consistent with Golgi staining, fine structures of CA3 neurons visualized by EGFP expression revealed no detectable alteration in terms of dendritic arborization and the distribution of presynaptic axonal boutons and postsynaptic spines (Fig. 5).

Immunoreactivities for postsynaptic proteins, PSD-95 and GluRα1/GluR1, were comparable in the hippocampal CA3 region between the two genotypes (Fig. 4D and E). Distribution of interneurons in the hippocampal CA3 and hilar areas was also indistinguishable as judged by immunostaining for GAD proteins (Fig. 4F), parvalbumin, somatostatin and calretinin. Thus, the histological and cytological organizations of the hippocampal CA3 region were indistinguishable between control and mutant mice.

Characteristic EEG spikes associated with multiple unit activities in the hippocampal CA3 region of mutant mice

Since seizure is produced by synchronous firing of a population of neurons in the brain [38], it is possible that NMDA receptor ablation in the CA3 region may modify hippocampal network oscillations *in vivo*. By recording local field potentials *in vivo* from the hippocampal CA3 region of urethane-anaesthetized mutant mice at the age of postnatal 8 weeks, we found characteristic spikes with large amplitudes (1.5–4.0 mV) (Fig. 6A). These EEG spikes were consistently observed in all 6 mutant mice, but never detected in 7 control mice. The mean firing rate of the spikes ($n=136$ from 6 mice) was 0.23 ± 0.02 Hz and the distribution of interspike intervals showed a peak at 4.75 s (Fig. 6B).

To investigate the origin of characteristic EEG spikes, we recorded field potentials in various hippocampal regions of mutant mice using a silicon probe with 16 recording sites. Simultaneous recording of a single EEG spike event from the hippocampal CA3 region and surrounding neocortex showed that the amplitude of EEG spikes was largest in the CA3 pyramidal cell layer. EEG spikes reversed their polarity in the CA3 stratum oriens (Fig. 6C). Current source density (CSD) analysis of EEG spikes revealed a current sink in the CA3 pyramidal cell layer, with a source nearby ($n=8$ from 4 mice). Recording from the cortex and hippocampal CA1 region, spikes reversed their polarity in the CA1 stratum oriens. CSD analyses revealed a large sink in the CA1 pyramidal cell layer ($n=8$ from 4 mice). On the other hand, EEG spikes recorded from the dentate gyrus showed neither polarity reversal nor sinks in CSD maps ($n=8$ from 4 mice). These results suggest that characteristic spikes are generated in the pyramidal cell layers of the CA3 and CA1 regions, but not in the dentate gyrus.

Further analysis revealed that the frequency of MUA in the CA3 pyramidal cell layer was enormously high during spike events (Fig. 6D, center). The strong correlation between MUA and EEG spikes was observed in all 4 mutant mice. After EEG spikes, MUA in the CA3 pyramidal cell layer became silent (Fig. 6D, center). MUA in the CA1 pyramidal cell layer were also associated with EEG spikes (Fig. 6D, right) and the association was reproducibly observed in all 4 mutant mice. On the other hand, there was no

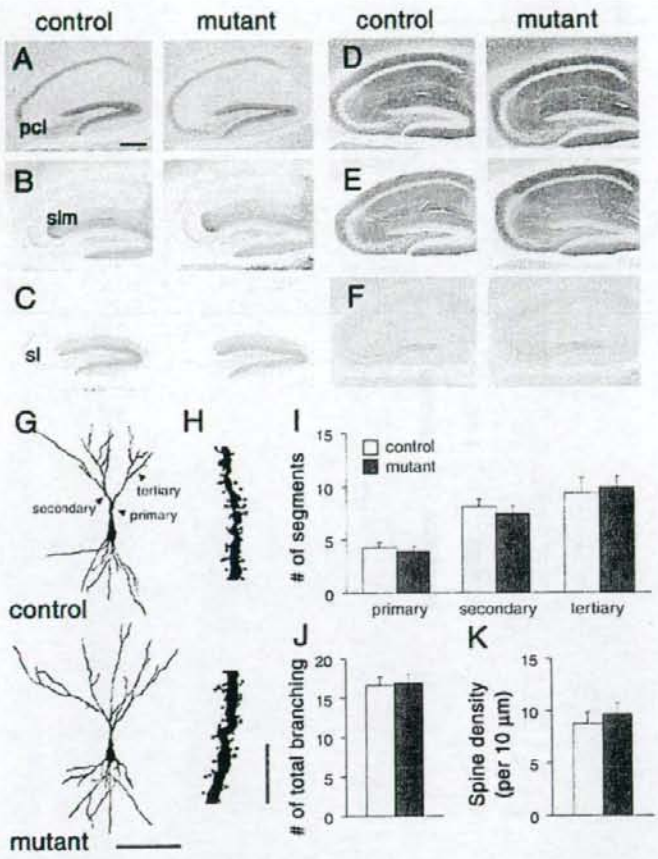

Figure 4. Normal histological organization of the hippocampal region. A, Nissl staining. **B, C,** Immunoperoxidase staining for VGluT2 (**B**) and Calbindin (**C**). **D–F,** Immunoperoxidase staining for PSD-95 (**D**), GluRα1 (**E**), and GAD (**F**). **G,** Cytoarchitecture of Golgi-stained CA3 pyramidal neurons. **H,** Higher magnification of the basal dendritic segment of CA3 pyramidal neuron in (**G**). **I–K,** Graphs represents the number of primary, secondary and tertiary dendrites (**I**), total number of dendritic branching (**J**), and spine density (**K**) of CA3 pyramidal neurons. Scale bars: **A**, 200 µm; **G**, 100 µm; **I**, 10 µm. Abbreviations: pcl, pyramidal cell layer; sl, stratum lucidum; slm, stratum lacunosum-moleculare.
doi:10.1371/journal.pone.0003993.g004

significant association in the dentate gyrus between MUA and spikes (Fig. 6D, left). The strong association of MUA with EEG spikes in the CA1 and CA3 pyramidal cell layers, but not in the dentate gyrus, together with CA3 pyramidal neuron-selective ablation of NMDA receptors, suggests that characteristic EEG spikes were originated from synchronous firing of CA3 pyramidal neurons and the activity of the CA3 network propagated to the downstream CA1 region.

Balanced excitatory and inhibitory synaptic transmission

Because either enhanced excitation or reduced inhibition can increase the excitability of hippocampal CA3 network, we examined the mRNA levels of excitatory glutamate receptor (GluR) subunits and glutamic acid decarboxylases (GADs) expressed in the hippocampal CA3 region of the mutant mice by *in situ* hybridization (Fig. 7A, Table 1). The *GluRζ1* mRNA was strongly diminished as described above. The reduction of the *GluRζ1* mRNA can be ascribed to the insertion of *cre* into one allele of the *GluRζ1* gene but the *cre* insertion exerted little effect on the kainate-induced seizure susceptibility as described above. There was no significant difference in the *GAD65* mRNA ($P=0.08$), while the level of *GAD67* mRNA was slightly but significantly reduced in the mutant mice ($P<0.001$). There were no significant differences in hybridization signals of other GluR mRNAs between control and mutant mice.

Basic electrophysiological properties of CA3 pyramidal cells were indistinguishable between two genotypes (resting membrane potential: control, -72.5 ± 0.8 mV, $n=32$; mutant -73.7 ± 1.0 mV, $n=26$, $P=0.37$; input resistance: control, 113.2 ± 5.3 MΩ; mutant, 117.7 ± 7.2 MΩ, $P=0.62$; membrane capacitance: control, 251.8 ± 9.4 pF; mutant, 250.2 ± 8.0 pF, $P=0.90$). We then compared $GABA_A$-IPSCs in the hippocampal CA3 region, which have been shown to suppress the excitability of the pyramidal cell through postsynaptic inhibition [39]. AMPA-EPSCs were evoked at −80 mV by stimulating afferent fibers in the CA3 stratum radiatum, which should activate both associa-

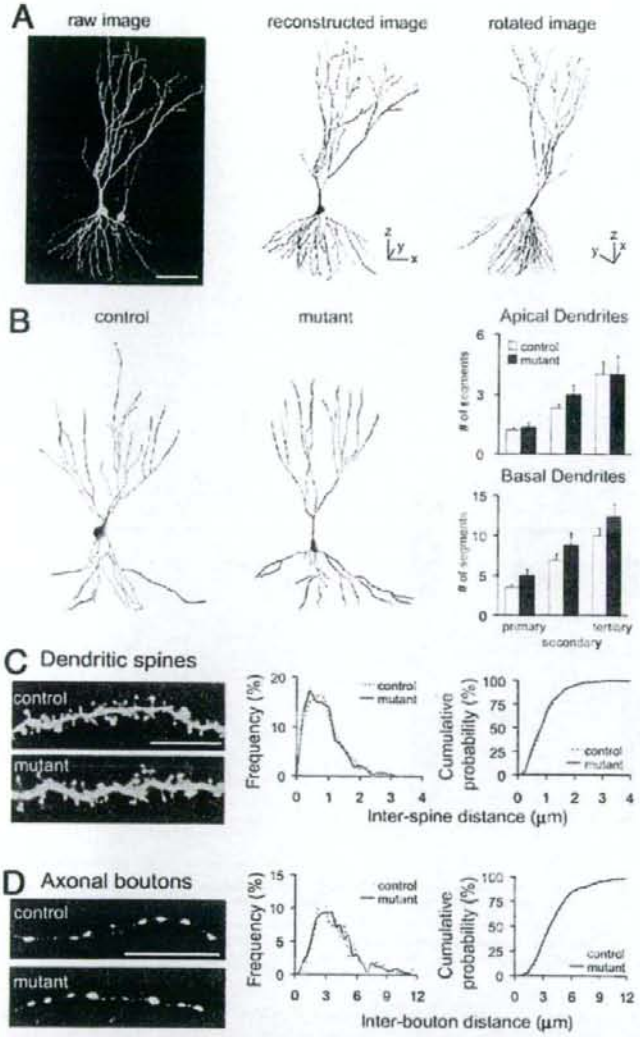

Figure 5. Dendritic branching and distribution of postsynaptic spines and presynaptic boutons in CA3 pyramidal neurons of control and mutant mice. A, Examples of three-dimensional reconstruction using IMARIS and FilamentTracer software. **B**, Three-dimensional reconstruction of AAV-EGFP-infected CA3 pyramidal neurons. Graphs represent the numbers of primary, secondary and tertiary dendrites of CA3 pyramidal neurons in control (open boxes, $n = 10–12$) and mutant mice (filled boxes, $n = 6–7$). There were no significant differences between control and mutant mice in the numbers of primary (apical, $P = 0.58$; basal, $P = 0.06$; t-test), secondary ($P = 0.13$, $P = 0.21$) and tertiary dendrites ($P = 1.0$ $P = 0.16$). **C**, Tertiary dendritic segments in control (left, top) and mutant (left, bottom) mice. Normalized distribution of inter-spine distances (middle, bin size, 0.1 μm). Cumulative distribution of inter-spine distances (right, same data set). There were no significant differences in inter-spine intervals of CA3 pyramidal neurons between two genotypes (control $n = 428$ from 10 dendrites of 4 mice; mutant, $n = 459$ from 9 dendrites of 4 mice; $P = 0.74$, Kolmogorov-Smirnov test). **D**, Boutons on the axon in the CA3 stratum radiatum of control (left, top) and mutant (left, bottom) mice. Normalized distribution of inter-bouton distances (middle, bin size, 0.4 μm). Cumulative distribution of inter-bouton distances (right, same data set). There were no significant differences in inter-bouton intervals of CA3 pyramidal neurons between two genotypes (control $n = 262$ from 18 axons of 4 mice; mutant, $n = 322$ from 24 dendrites of 4 mice; $P = 0.90$, Kolmogorov-Smirnov test).
doi:10.1371/journal.pone.0003993.g005

tional/commissural fibers and inhibitory interneurons (and their dendrites and axons), and then $GABA_A$-IPSCs were measured with the same stimulus strength at 0 mV in the presence of both the non-NMDA receptor antagonist CNQX and the NMDA receptor antagonist D-APV. The ratio of $GABA_A$-IPSCs to AMPA-EPSCs was indistinguishable between the two genotypes

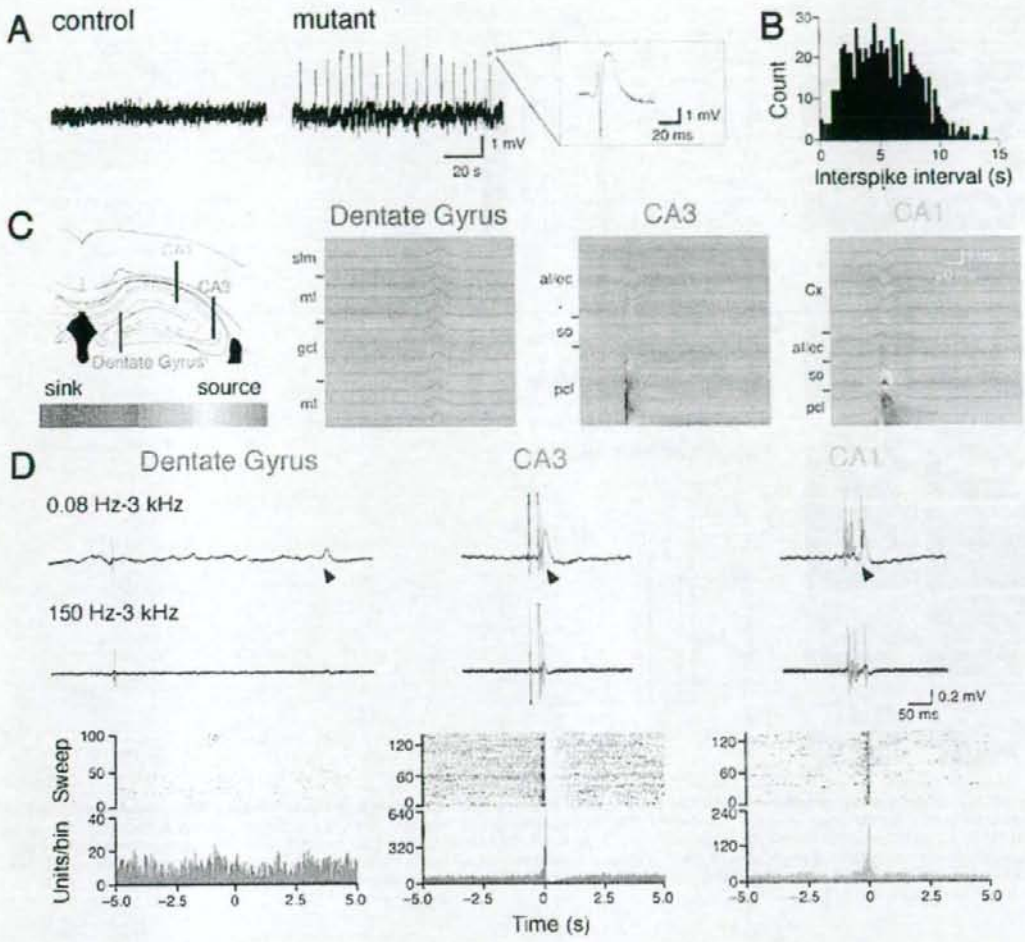

Figure 6. Characteristic large EEG spikes in the hippocampal CA3 region of mutant mice. A, Representative local field potential recordings from the CA3 region. **B**, Histogram of interspike intervals (bin, 0.25 s). **C**, Laminar profiles of field potentials and CSD analysis. Recording positions are illustrated on the left. Sinks and sources are indicated by cold and warm colors, respectively. Abbreviations: al/ec, alveus and external capsule; Cx, cortex; gcl, granule cell layer; ml, molecular layer; pcl, pyramidal cell layer; slm, stratum lacunosum-moleculare; so, stratum oriens. **D**, Wide-band recordings of extracellular activities (top), filtered MUA (middle) and raster plots and peri-event time histograms between MUA (bin, 200 ms) and EEG spikes in the dentate gyrus (left), CA3 (center) and CA1 regions (right). Arrowheads indicate the onset of spikes. MUA were aligned to the onset of spikes (time 0).
doi:10.1371/journal.pone.0003993.g006

(control, 0.52±0.09; mutant, 0.61±0.16; $n=12$ each; t-test, $P=0.65$) (Fig. 7B). Thus, there was no significant electrophysiological imbalance between AMPA receptor-mediated excitatory and $GABA_A$ receptor-mediated inhibitory synaptic transmission in the hippocampal CA3 region.

High-frequency stimulation failed to induce slow hyperpolarizing currents in hippocampal CA3 pyramidal neurons of mutant mice

In hippocampal CA1 pyramidal neurons, synaptic excitation is followed by an early GABA-mediated hyperpolarization and late AHP mediated by Ca^{2+}-dependent K^+ channels [40]. We thus examined the effect of NMDA receptor ablation on Ca^{2+}-dependent K^+ channels in hippocampal CA3 neurons. At a holding potential of −20 mV, high-frequency stimulation, which should activate both AMPA receptors and NMDA receptors in normal mice, induced slowly decaying outward currents in the pyramidal cells of control mice (Fig. 7C; peak amplitude, 46.1±5.4 pA, $n=12$). In contrast, such slow outward currents were hardly evoked by the same high-frequency stimulation in mutant mice (Fig. 7C; 0.5±2.1 pA, $n=12$, $P<0.001$). The outward currents in control mice were abolished by D-APV (Fig. 7D; control, 46.13±5.36 pA, $n=13$; D-APV, 0.38±2.41 pA, $n=12$,

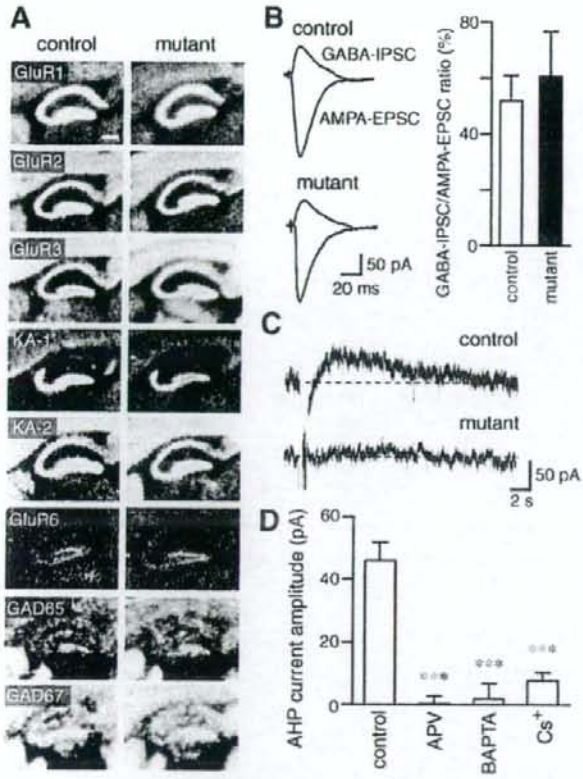

Figure 7. High-frequency stimulation failed to induce slow hyperpolarizing currents in hippocampal CA3 pyramidal neurons of mutant mice. **A**, X-ray film autoradiography for mRNAs of AMPA receptors, kainate receptors, and GADs. Scale bar, 200 μm. **B**, Representative traces of AMPA-EPSCs and $GABA_A$-IPSCs in the CA3 pyramidal cells. Graph shows the ratio of $GABA_A$-IPSCs to AMPA-EPSCs. **C**, Representative traces of slow hyperpolarizing currents. **D**, Peak amplitudes of the slow hyperpolarizing currents of the control mice in the absence (control) or presence of D-APV. Those recorded with a BAPTA-containing (BAPTA) or Cs^+-based internal solution (Cs^+) are also shown. ***, $P<0.001$, *t*-test.
doi:10.1371/journal.pone.0003993.g007

Table 1. Ratios of hybridization signal densities of GluR and GAD mRNAs in the CA3 region to those in the CA1 region.

mRNA	Control	Mutant
GluR(.1/NR1	0.86±0.02 ($n=10$)	0.04±0.01 ($n=5$)
GluRα1/GluR1	0.98±0.02 ($n=10$)	0.95±0.01 ($n=12$)
GluRα2/GluR2	0.91±0.03 ($n=8$)	0.89±0.03 ($n=11$)
GluRα3/GluR3	0.88±0.02 ($n=10$)	0.86±0.02 ($n=12$)
GluRγ2/KA-2	1.16±0.03 ($n=9$)	1.17±0.02 ($n=10$)
GluRβ2/GluR6	1.11±0.09 ($n=8$)	1.19±0.04 ($n=8$)
GAD65	1.12±0.05 ($n=10$)	0.99±0.05 ($n=11$)
GAD67	1.11±0.02 ($n=10$)	0.94±0.03 ($n=12$)

Slices were prepared from 3 mice of both genotypes.
Hybridization signal densities of the *GluRγ1/KA-1* mRNA in the CA3 region were 51.5±0.8 ($n=10$) in control mice and 32.3±0.5 ($n=12$) in mutant mice.
doi:10.1371/journal.pone.0003993.t001

$P<0.001$), suggesting that NMDA receptors are required for the response. NMDA receptor activation results in influx of Ca^{2+} into postsynaptic cells, which would activate Ca^{2+}-dependent K^+ channels. In fact, inclusion of the Ca^{2+} chelator BAPTA in the internal solution of patch pipettes diminished the outward currents (Fig. 7D; BAPTA, 1.99±4.76 pA, $n=7$, $P<0.001$). The outward currents were also diminished when recorded with a Cs^+-based internal solution (Fig. 7D; Cs^+, 7.74±2.35 pA, $n=4$, $P<0.001$), suggesting that the currents were mediated by postsynaptic K^+ channels. Taken together, the slow kinetics and sensitivities to D-APV, BAPTA and Cs^+ of the outward hyperpolarizing currents suggest that the high-frequency stimulation evokes slow AHP currents [41,42] mediated by Ca^{2+}-activated K^+ channels, which are activated by Ca^{2+} influx through NMDA receptor channels. These results suggest that the NMDA receptor-slow AHP coupling is diminished in the hippocampal CA3 pyramidal neurons of mutant mice, which may result in enhanced excitability of the CA3 recurrent network as a whole. The coupling between NMDA receptors and AHP currents is found in various regions [34,43–45]. However, the durations of AHP currents observed in our

experiment were much longer than those observed in previous studies.

These results with hippocampal CA3-specific NMDA receptor mutant mice raise an intriguing possibility that MDA receptors suppress the excitability of the CA3 recurrent network as a whole by restricting synchronous firing of CA3 neurons, although the possibility cannot be excluded that the enhanced excitability of the mutant mice might be due to subtle cytoarchitectural abnormalities of CA3 pyramidal neurons. To test the possibility, we then examined the effect of NMDA receptor ablation in the CA3 region of the adult brain on hippocampal network oscillations by employing a virus-mediated gene knockout technique [22,23].

Ablation of CA3 NMDA receptors in the mature brain also generated characteristic EEG spikes with large amplitudes

An adeno-associated viral expression vector for Cre recombinase (AAV-Cre, titer of $5–8 \times 10^{10}$) was stereotaxically microinjected to the hippocampal CA3 region of *GluRζ1*$^{flox/flox}$ mice at 8–9 weeks old. Immunohistochemical analysis revealed that the infection of AAV-Cre was limited to the hippocampal CA3 region and spread within 40–70% of the region (Fig. 8A–C). Immunoreactivity for GluRζ1 was diminished in the well-demarcated infected CA3 region by 2 weeks after infection (Fig. 8C). Age-matched *GluRζ1*$^{+/+}$ mice microinjected with AAV-Cre served as controls.

Local field potential recording from the CA3 region showed characteristic EEG spikes with large amplitudes in *GluRζ1*$^{flox/flox}$ mice 2–3 weeks after AAV-Cre infection ($n = 5$ out of 9 mice) (Fig. 8D). The frequency of large EEG spikes was variable among subjects, which may be related to the variance of AAV-infected regions among animals. No such spike activity was detected in EEG records from the CA3 region of AAV-Cre-infected *GluRζ1*$^{+/+}$ mice ($n = 7$ out of 7 mice, $P = 0.02$, Fisher's exact probability test) (Fig. 8D). CSD analysis revealed the sink in the pyramidal cell layer of the CA3 region and the sources in neighboring stratum oriens (Fig. 8E, $n = 8$ spikes). Thus, the ablation of CA3 NMDA receptors induced by AAV-Cre infection in the adult brain also resulted in the generation of characteristic EEG spikes.

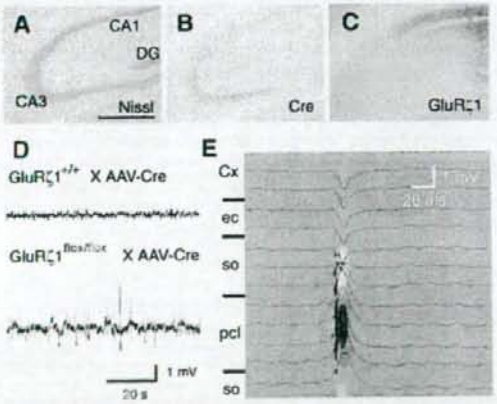

Figure 8. Hippocampal CA3 NMDA receptor ablation in the adult brain also generated characteristic EEG spikes with large amplitudes. A–C, AAV-Cre-mediated ablation of NMDA receptors in the hippocampal CA3 region. Nissl staining (**A**) and imunohistochemistry for Cre (**B**) and GluRζ1 (**C**). Scale bar, 0.5 mm. **D**, Representative local field potential recordings from the CA3 region. **E**, Laminar profiles of field potentials and CSD analysis. Recording positions are illustrated on the left. Sinks and sources are indicated by cold and warm colors, respectively. Cx, cortex; ec, external capsule; pcl, pyramidal cell layer; so, stratum oriens.

doi:10.1371/journal.pone.0003993.g008

Pharmacological blockade of CA3 NMDA receptors enhanced the susceptibility to kainate-induced seizure

We finally examined the seizure susceptibility of wild-type mice by focal injection of a competitive NMDA receptor antagonist, APV. We bilaterally injected 30 mM APV or aCSF into the hippocampal CA3 region of C57BL/6N mice at postnatal 8–10 weeks. About 20–30 minutes later, the animals were intraperitoneally administrated with the convulsive dose of kainate (30 mg/kg) [46]. Kainate-induced tonic-clonic seizures with loss of the postural tone appeared within 1 h in both groups of mice ($n = 8$ each; $P = 0.23$, Fisher's exact probability test) (Fig. 9). However, the latency to the onset of seizures was significantly shorter in mice injected with APV ($n = 8$; $P = 0.0044$, Log-rank test). Thus, the focal blockage of CA3 NMDA receptors also enhanced the susceptibility to kainate-induced seizure.

Discussion

Here, we generated hippocampal CA3 pyramidal neuron-specific NMDA receptor mutant mice on the C57BL/6N genetic background. The expression of the *GluRζ1* mRNA was comparable between mutant and control mice at P1 but strongly decreased in mutant mice at P7. The significant expression of GluRζ1 protein, though reduced, was found in the CA3 region at P7 but diminished to a negligible level by P14. We found that the mutant mice lacking NMDA receptors in the hippocampal CA3 pyramidal neurons showed enhanced susceptibility to kainate-induced seizures. This observation was rather unexpected since NMDA receptor-mediated LTP was implied to contribute to the generation of synchronous network activity by *in vitro* studies [14,15]. We found that characteristic EEG spikes with large amplitude were generated by the ablation of NMDA receptors in CA3 pyramidal neurons. Strong association of MUA with the characteristic EEG spikes in the CA3 pyramidal cell layer of mutant mice suggests that the CA3 NMDA receptor ablation increases the synchronous network activity possibly by affecting the firing pattern of CA3 neurons. In contrast, CA1 region-specific ablation of NMDA receptors appeared to hardly affect EEG *in vivo* [47]. NMDA receptor antagonists have minimal effects on basal synaptic transmission but completely block the generation of long-term potentiation in the CA1 region *in vitro* [48–50]. Hence, NMDA receptors in the CA1 region are not considered to be involved in spontaneous network activity. The difference in the neural wiring pattern such as the abundance of recurrent networks may underlie the different effects of NMDA receptor ablation in the hippocampal CA1 and CA3 regions on network activity. Our results raise an intriguing possibility that NMDA receptors may suppress the excitability of the CA3 network as a whole *in vivo*.

It is possible that the ablation of NMDA receptors may disturb the neural wiring of the hippocampal CA3 region, leading to abnormal excitability of the network. It is well known that the NMDA receptor plays a role in the activity-dependent refinement of synaptic connections and neural pattern formation [51–54]. Chronic blockade of NMDA receptors in hippocampal slice cultures during the first two weeks of postnatal development leads to a substantial increase in synapse number and results in a more complex dendritic arborization of CA1 pyramidal cells [31]. The activity blockade in hippocampus during postnatal 2–3 weeks by

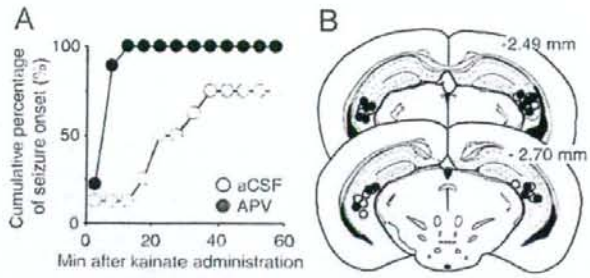

Figure 9. The pharmacological blockade of CA3 NMDA receptors increased the susceptibility to kainate-induced seizures. A, Cumulative curves for the onset of seizure. **B,** Illustration of the injection sites of APV (filled) and aCSF (open). Numbers represent distance (mm) of the section relative to the bregma landmark.
doi:10.1371/journal.pone.0003993.g009

tetrodotoxin infusion produced both behavioral and electrographic seizures 2 weeks after the infusion [55] and the increase in the density of axonal varicosities and postsynaptic AMPA receptor GluR1 and NMDA receptors [56]. Thus, reduced neuronal activity during development might potentially enhance the excitability. However, the cytoarchitecture was indistinguishable between control and mutant mice at P21–23. There were no detectable differences in the dendritic branching and the density of axonal boutons and dendritic spines between control and mutant mice at P21–23. The sustained expression of NMDA receptor proteins at least by P7 in mutant mice may support the development of CA3 pyramidal neuron cytoarchitectures. An alternative possibility is that the excitability of the CA3 network may be suppressed by NMDA receptor-mediated signaling. No significant differences were detectable in the basic membrane properties and balance between excitatory and inhibitory synaptic transmission between control and mutant mice. At synapses, activation of NMDA receptors evokes excitatory postsynaptic potential on the CA3 pyramidal neurons *in vitro* [57]. However, the enhancement of the kainate-induced seizure susceptibility and the emergence of characteristic EEG spikes associated with MUA in the mutant mice can be hardly explained if major roles of NMDA receptors would be simply mediating and strengthening the excitatory transmission at the commissural/associational synapses. Besides excitatory transmission and its enhancement, NMDA receptors may mediate diverse suppressive signals including spike-timing dependent long-term depression [58], LTP of slow GABA-IPSCs [59], the increase in I_h currents [60], and coupling with K^+ channels [34,43–45]. Thus, it is possible that NMDA receptor signaling may suppress the excitability of the CA3 network *in vivo*, although the possibility cannot be excluded that the enhanced excitability of the mutant mice might be due to subtle developmental abnormalities of CA3 pyramidal neurons.

We thus examined whether the excitability of the CA3 network is enhanced by ablation of NMDA receptors in the adult brain with a virus-mediated gene knockout technique [22,23]. We found that EEG spikes with large amplitude were generated by focal ablation of NMDA receptors in the CA3 region of adult mice by AAV-Cre infection. The frequency of large EEG spikes was variable among subjects, which may be related to the variance of AAV-infected regions among animals. Furthermore, the blockade of NMDA receptors by focal injection of APV into the hippocampal CA3 region enhanced the susceptibility to kainate-induced seizures. These results suggest that NMDA receptors control negatively the excitability of the hippocampal CA3 recurrent network as a whole *in vivo* by restricting synchronous firing of CA3 neurons, although the mechanism remains to be solved. Since slow AHP currents are involved in accommodation of action potential discharge of CA1 pyramidal neurons [40], it is possible that the frequency of action potentials may increase in a mutant CA3 pyramidal neuron where NMDA receptor-AHP coupling is eliminated. Prolonged discharges of CA3 pyramidal neurons might increase the chance of their synchronous firing, leading to the enhancement of the excitability of the CA3 network as a whole. Interestingly, Colgin et al. reported that blockade of NMDA receptors enhanced spontaneous sharp waves in rat hippocampal slices [61], supporting the idea that activation of NMDA receptors can serve to dampen the excitation of sharp waves. On the other hand, studies through computational models showed that when recurrent networks with conductance delays exhibit population bursts, spike-timing-dependent plasticity (STDP) rules exert a strong decoupling force that desynchronizes activity [58]. Thus, elimination of NMDA receptor-dependent STDP might enhance synchronization in CA3 recurrent networks. One or combination of such NMDA receptor-mediated suppressive signals [34,43–45,58–60] might underlie the regulation of CA3 network excitability. The NMDA receptors in the hippocampal CA3 region are implied in rapid acquisition and recall of associative memory as well as paired associate learning [11–13]. These functions may be mediated not only by the plasticity at synapses but also by the NMDA receptor-mediated neural network oscillation.

Acknowledgments

We thank Dr. H. Kashiwadani and Dr. K. Mori for valuable advice and help in field potential recordings and critical reading of the manuscript, Dr. Y. Kiyama for help in targeting vector construction, Ms R. Natsume for chimeric mouse preparation, Ms E. Kato for advice on Golgi staining, Mrs N. Takino and H. Nishida for technical assistance in AAV vector production, Ms A. Kishioka for help in animal surgery, Dr. T. Takeuchi for help in ES cell preparation, and Mrs H. Wakamatsu, Y. Takushi and T. Kurokawa for help in mice breeding. We are grateful to Dr. M. Ohtsuka for his encouragement and support. Thanks are also to Drs H. Iwama, I. Ito, Y. Takahashi and T. Tsujimoto for advice.

Author Contributions

Conceived and designed the experiments: FF KN MW TM MM. Performed the experiments: FF KN TS MF MW. Analyzed the data: FF KN TS MF MW. Contributed reagents/materials/analysis tools: SiM KS HK HM. Wrote the paper: FF KN MW TM MM.

References

1. Amaral DG, Witter MP (1989) The three-dimensional organization of the hippocampal formation: a review of anatomical data. Neuroscience 31: 571–591.
2. MacVicar BA, Dudek FE (1980) Local synaptic circuits in rat hippocampus: interactions between pyramidal cells. Brain Res 184: 220–223.
3. Miles R, Wong RK (1983) Single neurones can initiate synchronized population discharge in the hippocampus. Nature 306: 371–373.
4. Traub RD, Miles R (1991) Collective behaviours of the CA3 network: experiment and model. Neuronal Networks of The Hippocampus. Cambridge: Cambridge University Press. pp 119–156.
5. Buzsáki G (1989) Two-stage model of memory trace formation: a role for "noisy" brain states. Neuroscience 31: 551–570.
6. Jefferys JGR (1993) The pathophysiology of epilepsies. In: Laidlaw J, Richens A, Chadwick D, eds. A Textbook of epilepsy. 4th ed. Edinburgh: Churchill Livingstone. pp 241–276.
7. Csicsvari J, Hirase H, Czurko A, Buzsáki G (1998) Reliability and state dependence of pyramidal cell-interneuron synapses in the hippocampus: an ensemble approach in the behaving rat. Neuron 21: 179–189.
8. Ylinen A, Bragin A, Nádasdy Z, Jandó G, Szabó I, et al. (1995) Sharp wave-associated high-frequency oscillation (200 Hz) in the intact hippocampus: network and intracellular mechanisms. J Neurosci 15: 30–46.
9. Morris RG (2003) Long-term potentiation and memory. Philos Trans R Soc Lond B Biol Sci 358: 643–647.
10. Jonas P, Major G, Sakmann B (1993) Quantal components of unitary EPSCs at the mossy fibre synapse on CA3 pyramidal cells of rat hippocampus. J Physiol 472: 615–663.
11. Nakazawa K, Quirk MC, Chitwood RA, Watanabe M, Yeckel MF, et al. (2002) Requirement for hippocampal CA3 NMDA receptors in associative memory recall. Science 297: 211–218.
12. Nakazawa K, Sun LD, Quirk MC, Rondi-Reig L, Wilson MA, et al. (2003) Hippocampal CA3 NMDA receptors are crucial for memory acquisition of one-time experience. Neuron 38: 305–315.
13. Rajji T, Chapman D, Eichenbaum H, Greene R (2006) The role of CA3 hippocampal NMDA receptors in paired associate learning. J Neurosci 26: 908–915.
14. Bains JS, Longacher JM, Staley KJ (1999) Reciprocal interactions between CA3 network activity and strength of recurrent collateral synapses. Nat Neurosci 2: 720–726.
15. Behrens CJ, van den Boom LP, de Hoz L, Friedman A, Heinemann U (2005) Induction of sharp wave-ripple complexes in vitro and reorganization of hippocampal networks. Nat Neurosci 8: 1560–1567.
16. Yamazaki M, Mori H, Araki K, Mori KJ, Mishina M (1992) Cloning, expression and modulation of a mouse NMDA receptor subunit. FEBS Lett 300: 39–45.
17. Taniguchi M, Yuasa S, Fujisawa H, Naruse I, Saga S, et al. (1997) Disruption of semaphorin III/D gene causes severe abnormality in peripheral nerve projection. Neuron 19: 519–530.
18. Takeuchi T, Miyazaki T, Watanabe M, Mori H, Sakimura K, et al. (2005) Control of synaptic connection by glutamate receptor δ2 in the adult cerebellum. J Neurosci 25: 2146–2156.
19. Mishina M, Sakimura K (2007) Conditional gene targeting on the pure C57BL/6 genetic background. Neurosci Res 58: 105–112.
20. Takeuchi T, Nomura T, Tsujita M, Suzuki M, Fuse T, et al. (2002) Flp recombinase transgenic mice of C57BL/6 strain for conditional gene targeting. Biochem Biophys Res Commun 293: 953–957.
21. Werner P, Voigt M, Keinanen K, Wisden W, Seeburg PH (1991) Cloning of a putative high-affinity kainate receptor expressed predominantly in hippocampal CA3 cells. Nature 351: 742–744.
22. Li XG, Okada T, Kodera M, Nara Y, Takino N, et al. (2006) Viral-mediated temporally controlled dopamine production in a rat model of Parkinson disease. Mol Ther 13: 160–166.
23. Scammell TE, Arrigoni E, Thompson MA, Ronan PJ, Saper CB, et al. (2003) Focal deletion of the adenosine A1 receptor in adult mice using an adeno-associated viral vector. J Neurosci 23: 5762–5770.
24. Fukaya M, Kato A, Lovett C, Tonegawa S, Watanabe M (2003) Retention of NMDA receptor NR2 subunits in the lumen of endoplasmic reticulum in targeted NR1 knockout mice. Proc Natl Acad Sci U S A 100: 4855–4860.
25. Miyazaki T, Fukaya M, Shimizu H, Watanabe M (2003) Subtype switching of vesicular glutamate transporters at parallel fibre-Purkinje cell synapses in developing mouse cerebellum. Eur J Neurosci 17: 2563–2572.
26. Nakagawa S, Watanabe M, Isobe T, Kondo H, Inoue Y (1998) Cytological compartmentalization in the staggerer cerebellum, as revealed by calbindin immunohistochemistry for Purkinje cells. J Comp Neurol 395: 112–120.
27. Fukaya M, Watanabe M (2000) Improved immunohistochemical detection of postsynaptically located PSD-95/SAP90 protein family by protease section pretreatment: a study in the adult mouse brain. J Comp Neurol 426: 572–586.
28. Shimuta M, Yoshikawa M, Fukaya M, Watanabe M, Takeshima H, et al. (2001) Postsynaptic modulation of AMPA receptor-mediated synaptic responses and LTP by the type 3 ryanodine receptor. Mol Cell Neurosci 17: 921–930.
29. Yamada K, Fukaya M, Shimizu H, Sakimura K, Watanabe M (2001) NMDA receptor subunits GluRε1, GluRε3 and GluRζ1 are enriched at the mossy fibre-granule cell synapse in the adult mouse cerebellum. Eur J Neurosci 13: 2025–2036.
30. Watanabe M, Fukaya M, Sakimura K, Manabe T, Mishina M, et al. (1998) Selective scarcity of NMDA receptor channel subunits in the stratum lucidum (mossy fibre-recipient layer) of the mouse hippocampal CA3 subfield. Eur J Neurosci 10: 478–487.
31. Luthi A, Schwyzer L, Mateos JM, Gahwiler BH, McKinney RA (2001) NMDA receptor activation limits the number of synaptic connections during hippocampal development. Nat Neurosci 4: 1102–1107.
32. Fukaya M, Yamazaki M, Sakimura K, Watanabe M (2005) Spatial diversity in gene expression for VDCCγ subunit family in developing and adult mouse brains. Neurosci Res 53: 376–383.
33. Yamada K, Fukaya M, Shibata T, Kurihara H, Tanaka K, et al. (2000) Dynamic transformation of Bergmann glial fibers proceeds in correlation with dendritic outgrowth and synapse formation of cerebellar Purkinje cells. J Comp Neurol 418: 106–120.
34. Isaacson JS, Murphy GJ (2001) Glutamate-mediated extrasynaptic inhibition: direct coupling of NMDA receptors to Ca^{2+}-activated K^+ channels. Neuron 31: 1027–1034.
35. Murakami M, Kashiwadani H, Kirino Y, Mori K (2005) State-dependent sensory gating in olfactory cortex. Neuron 46: 285–296.
36. Franklin KBJ, Paxinos G (1996) The mouse brain in stereotaxic coordinates. San Diego: Academic Press.
37. Ben-Ari Y (1985) Limbic seizure and brain damage produced by kainic acid: mechanisms and relevance to human temporal lobe epilepsy. Neuroscience 14: 375–403.
38. Westbrook GL (2000) Seizures and Epilepsy. In: Kandel ER, Schwartz JH, Jessell TM, eds. Principles of Neural Science. 4th ed. Cambridge: Cambridge Univ Press. pp 910–935.
39. Lawrence JJ, McBain CJ (2003) Interneuron diversity series: containing the detonation—feedforward inhibition in the CA3 hippocampus. Trends Neurosci 26: 631–640.
40. Nicoll RA, Alger BE (1981) Synaptic excitation may activate a calcium-dependent potassium conductance in hippocampal pyramidal cells. Science 212: 957–959.
41. Schwartzkroin PA, Stafstrom CE (1980) Effects of EGTA on the calcium-activated afterhyperpolarization in hippocampal CA3 pyramidal cells. Science 210: 1125–1126.
42. Stocker M, Krause M, Pedarzani P (1999) An apamin-sensitive Ca^{2+}-activated K^+ current in hippocampal pyramidal neurons. Proc Natl Acad Sci U S A 96: 4662–4667.
43. Faber ES, Delaney AJ, Sah P (2005) SK channels regulate excitatory synaptic transmission and plasticity in the lateral amygdala. Nat Neurosci 8: 635–641.
44. Lin MT, Lujan R, Watanabe M, Adelman JP, Maylie J (2008) SK2 channel plasticity contributes to LTP at Schaffer collateral-CA1 synapses. Nat Neurosci 11: 170–177.
45. Ngo-Anh TJ, Bloodgood BL, Lin M, Sabatini BL, Maylie J, et al. (2005) SK channels and NMDA receptors form a Ca^{2+}-mediated feedback loop in dendritic spines. Nat Neurosci 8: 642–649.
46. Mulle C, Sailer A, Pérez-Otaño I, Dickinson-Anson H, Castillo PE, et al. (1998) Altered synaptic physiology and reduced susceptibility to kainate-induced seizures in GluR6-deficient mice. Nature 392: 601–605.
47. McHugh TJ, Blum KI, Tsien JZ, Tonegawa S, Wilson MA (1996) Impaired hippocampal representation of space in CA1-specific NMDAR1 knockout mice. Cell 87: 1339–1349.
48. Bear MF, Malenka RC (1994) Synaptic plasticity: LTP and LTD. Curr Opin Neurobiol 4: 389–399.
49. Bliss TV, Collingridge GL (1993) A synaptic model of memory: long-term potentiation in the hippocampus. Nature 361: 31–39.
50. Malenka RC, Nicoll RA (1999) Long-term potentiation—a decade of progress? Science 285: 1870–1874.
51. Cline HT, Debski EA, Constantine-Paton M (1987) *N*-methyl-D-aspartate receptor antagonist desegregates eye-specific stripes. Proc Natl Acad Sci U S A 84: 4342–4345.
52. Kleinschmidt A, Bear MF, Singer W (1987) Blockade of "NMDA" receptors disrupts experience-dependent plasticity of kitten striate cortex. Science 238: 355–358.
53. Kutsuwada T, Sakimura K, Manabe T, Takayama C, Katakura N, et al. (1996) Impairment of suckling response, trigeminal neuronal pattern formation, and hippocampal LTD in NMDA receptor ε2 subunit mutant mice. Neuron 16: 333–344.
54. Li Y, Erzurumlu RS, Chen C, Jhaveri S, Tonegawa S (1994) Whisker-related neuronal patterns fail to develop in the trigeminal brainstem nuclei of NMDAR1 knockout mice. Cell 76: 427–437.
55. Galvan CD, Hrachovy RA, Smith KL, Swann JW (2000) Blockade of neuronal activity during hippocampal development produces a chronic focal epilepsy in the rat. J Neurosci 20: 2904–2916.
56. Galvan CD, Wenzel JH, Dineley KT, Lam TT, Schwartzkroin PA, et al. (2003) Postsynaptic contributions to hippocampal network hyperexcitability induced by chronic activity blockade in vivo. Eur J Neurosci 18: 1861–1872.

57. Debanne D, Gähwiler BH, Thompson SM (1998) Long-term synaptic plasticity between pairs of individual CA3 pyramidal cells in rat hippocampal slice cultures. J Physiol 507: 237–247.
58. Lubenov EV, Siapas AG (2008) Decoupling through synchrony in neuronal circuits with propagation delays. Neuron 58: 118–131.
59. Huang CS, Shi SH, Ule J, Ruggiu M, Barker LA, et al. (2005) Common molecular pathways mediate long-term potentiation of synaptic excitation and slow synaptic inhibition. Cell 123: 105–118.
60. Fan Y, Fricker D, Brager DH, Chen X, Lu HC, et al. (2005) Activity-dependent decrease of excitability in rat hippocampal neurons through increases in I(h). Nat Neurosci 8: 1542–1551.
61. Colgin LL, Jia Y, Sabatier J-M, Lynch G (2005) Blockade of NMDA receptors enhances spontaneous sharp waves in rat hippocampal slices. Neurosci Lett 385: 46–51.

厚生労働科学研究費補助金
創薬基盤推進研究事業（ヒトゲノムテーラーメード研究事業）

パーキンソン病遺伝子治療臨床研究における安全性評価と
positron emission tomography(PET)による有効性の評価
平成１８年度～２０年度　総合研究報告書

発　　行　平成２１年３月３１日
研究代表者　中　野　今　治
栃木県下野市薬師寺３３１１－１
自治医科大学医学部神経内科